Simulation of Start-Up Behaviour of Induction Motor with Direct Online Connection

Stanislav KOCMAN, Petr ORSAG, Pavel PECINKA

Department of Electrical Engineering, Faculty of Electrical Engineering and Computer Science, VSB–Technical university of Ostrava, 17. listopadu 15, 708 33 Ostrava, Czech Republic

stanislav.kocman@vsb.cz, petr.orsag@vsb.cz, pavel.pecinka@vsb.cz

DOI: 10.15598/aeee.v15i5.2342

Abstract. *In this paper, a simulation of dynamical start-up behaviour of induction motor with direct online connection to the network has been carried out using COMSOL Multiphysics software. The simulated model of the motor mainly consists of a basic FEM model, an electrical model with stator and rotor circuits and a mechanical model. The chosen motor parameters both electrical and mechanical have been studied and their results presented in this paper. An experimental measurement of the start-up transient of the no-loaded motor was carried out and some its results have been compared to the results from the simulated motor model and analysed.*

Keywords

COMSOL, induction motor, model, simulation, start-up.

1. Introduction

The direct on line start-up of the three-phase squirrel cage induction motor is the common starting method in the industrial applications [1], [2] and [3]. Starting induction motor is a transient process from the motor standstill to its operating speed, during which the motor speed, currents in stator and rotor and torque change. At the moment of the motor connection to the mains, it behaves like a transformer with short-circuited secondary winding. The impedance of the motor at the standstill when the slip is equal to 1 is considerably lower than at the rotating rotor. Thus, the starting current is high. But it is less than the short-circuit current of a transformer due to higher stray of the induction motor [4] and [5]. The drawn starting current, e.g. at standard motors, is usually about 5 to 8 times the nominal motor current, but at some industrial applications with a hard start-up can be higher [6]. The value of the starting current depends on the motor design and size. The starting torque is also high, e.g. at the standard motors, it is about 2 to 3.5 times the motor nominal torque and depends on the motor design and size [7].

The direct online start-up has advantages of the simple equipment, low costs, high starting torque and eventually fast start. The limitation of this starting method is the high starting current causing a voltage drop in the power line, which can affect the operation of other devices connected to the mains [1], [2] and [3]. For this reason, there are limits for permissible powers of motors connected directly to the mains. However, they can vary in various types of the mains. High starting current also has negative impacts on the induction motor (forces acting on coil end and machine overheating due to often starting, reversing and braking). The starting torque, often higher than the driven machines need, can result in mechanical stresses in couplings and driven machines. To avoid the negative impacts of the direct online start-up, the motors of the rated power below 4–5 kW can be connected directly to the mains. Nevertheless, it can be higher if the motor rated power is low in comparison to the power of the mains, the starting torque does not affect the operation of driven machine or the driven machine does not need to speed up gradually. Otherwise, other starting methods are used described e.g. in [8] and [9].

Starting time is a function of motor torque, moment of inertia and load torque. Too long start-up can cause non-permissible temperature rise in the motor [10], [11] and [12], because the temperature depends on the product of the time and the square of the current, but also on the motor cooling condition. For this reason, the starting time must not exceed the time specified in the documentation of the manufacturer.

To simulate start-up behaviour of the induction motor directly connected to the mains the COMSOL Multiphysics has been used [13]. This software is based on the Finite Element Method (FEM), which is used to find solutions to various scientific and engineering problems. Thus, it is widely used to design and study electrical machines; it also means induction motors [14], [15] and [16].

The aim of this paper is to simulate motor parameters during the motor start-up at various conditions and a comparison of chosen parameters such as speed, currents and torque to their values from an experimental measurement.

2. Experimental Measurement of Motor Start-Up

The circuit diagram for the measurement of motor start-up is shown in Fig. 1. The tested induction motor, with catalogue parameters shown in Tab. 1, has been fed by the programmable power source Pacific 3120AMX enabling an adjustment of the motor nominal frequency and nominal voltage being almost purely harmonic with total harmonic distortion THD_U equal to 0.14 %. An external feedback was connected to the source to compensate the voltage drop in the cable from the source to the motor.

Tab. 1: The selected parameters of the motor.

Parameter	Value	Parameter	Value
Rated power	4 kW	Nom. power factor	0.83
Nominal voltage	400 V	Nominal speed	1440 rpm
Nominal current	8.4 A	Nominal torque	27 N·m
Starting current ratio	6	Starting torque ratio	2.7
Nominal frequency	50 Hz	Nominal efficiency	83.1

The torque and speed of the induction motor have been measured by the HBM T20WN50 transducer with the declared accuracy class of 0.2 %. The current clamps Chauvin Arnoux C35N were used for the measurement of the drawn currents. The induction motor was not loaded during its start-up, so the mechanically connected DC motor was not energized. The measurement of three phase voltages and currents, mechanical torque and speed has been carried out by a digital multi-channel measurement system with a sampling rate of 156.25 kSa·s^{-1}. The system is based on two National Instruments DAQ boards NI PCI-MIO16-E1, working in parallel and synchronized by the RTSI bus. The voltages were recorded by the first board, whereas currents, torque and speed were recorded by the second board. The isolation modules DAQP-HV-B were used for signal conditioning of the first board and isolation modules DAQP-LV-BNC were used for signal conditioning of the second board. All isolation modules, manufactured by Dewetron, are equipped with high precision signal conditioning amplifiers.

The measurement has been carried out with the no-loaded motor in the drive assembly as seen in Fig. 1 with the moment of inertia equal to 0.05 kg·m^2. The waveform of the currents drawn by the no-loaded motor from the source is shown in Fig. 2, the mechanical torque in Fig. 3 and the speed in Fig. 4. As seen, the start-up transient is fast when the steady-state speed is reached in c. 0.2 s. The negative values in the torque waveform are caused by the electromechanical coupling and a response of the motor on the start-up. These results will be compared to the results from a simulation model of the induction motor.

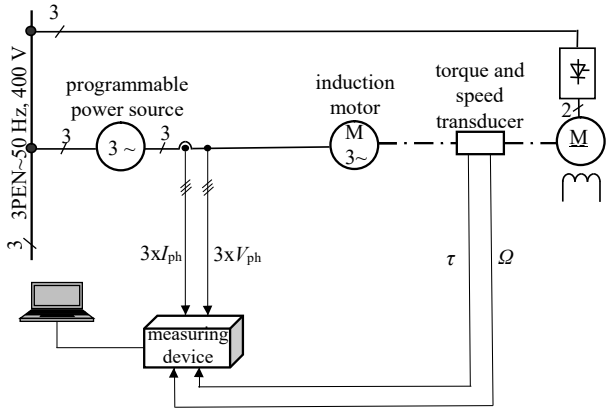

Fig. 1: Circuit diagram for the measurement of motor start-up.

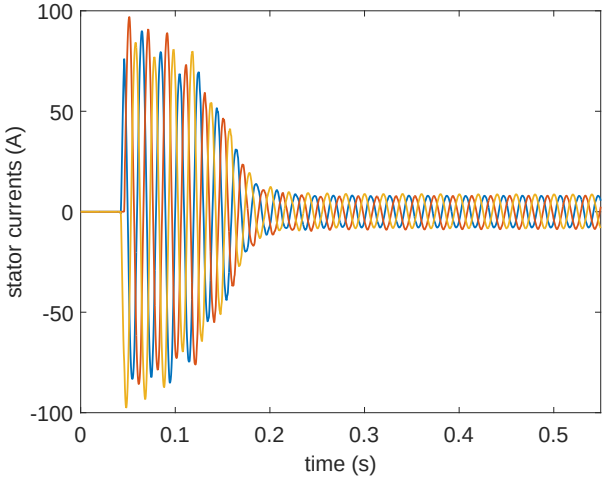

Fig. 2: Waveform of stator currents during start-up.

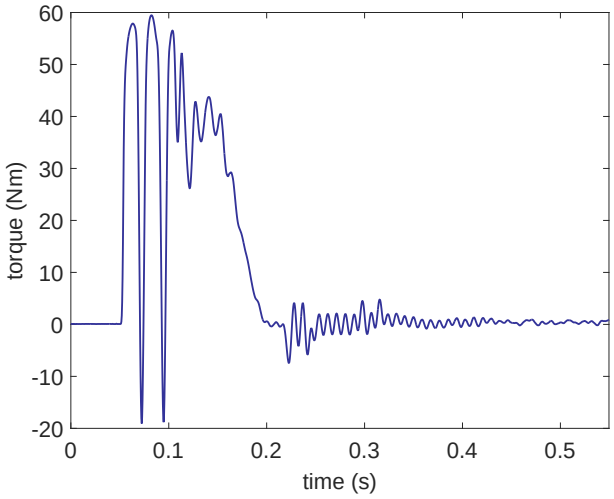

Fig. 3: Waveform of torque during start-up.

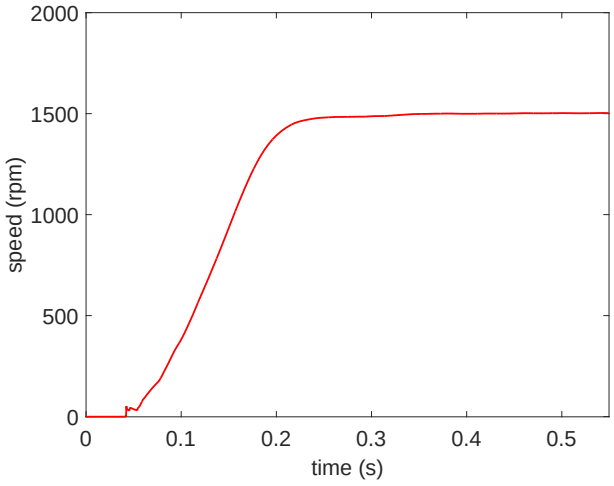

Fig. 4: Waveform of speed during start-up.

3. Model of Induction Motor

The measured induction motor was modelled in COMSOL as a two-dimensional model with defined out of plane thickness, i.e. as the quasi-3D model. For its design and analysis, the Rotating Machinery, Magnetic interface under the AC/DC Module is used [17]. This physics enables solving the magnetic field in the motor. The equations assuming time-dependent study of the magnetic field in the motor parts are defined as follows:

$$\sigma\frac{\partial A}{\partial t} + \nabla \times H - \sigma v \times B = J_e, \tag{1}$$

$$\nabla \times A = B, \tag{2}$$

where σ is the electric conductivity in (S·m^{-1}), A is the magnetic vector potential in (V·s·m^{-1}), H is the magnetic field intensity in (A·m^{-1}), v is the velocity of conductors in (m·s^{-1}), B is the magnetic flux density in (T), J_e is the externally generated current density in (A·m^{-2}).

For the stator slots the multi-turn coil domains are used, where the externally generated current density J_e is formulated as:

$$J_e = \frac{NI}{A}e, \tag{3}$$

where N is the number of turns of the stator coil, I is the stator phase current in (A), A is the total cross-section area of the stator coil domain in (m^2), e is the vector field representing the direction of the wires in the stator slot.

The rotor slots are defined using single-turn coil domains, where the externally generated current density for the time-dependent study is formulated as:

$$J_e = \sigma\frac{V}{d}e, \tag{4}$$

where V is the electrical potential applied on the turn of the coil, i.e. on the rotor bar in (V), d is the out of plane physics thickness in (m).

The motor inner torque τ computed by the integration of the Maxwell's stress tensor over the exterior surfaces of the set of domains is defined as:

$$\tau = \oint_{\partial\Omega} d(r - r_0) \times (nT)\mathrm{d}S, \tag{5}$$

where Ω is set of domains involving domains in the rotor, shaft and the half of the motor air gap, r is the position vector, r_0 is the torque rotation point, n is the outward normal from the surface, T is the stress tensor and dS represents the differential boundary length.

Starting induction motor in a drive assembly is a transient process, which is described by the fundamental torque equation, or the equation of motion, as follows:

$$\tau = \tau_L + j\frac{\mathrm{d}\omega}{\mathrm{d}t}, \tag{6}$$

where τ_L is the load torque in (N·m), J is the moment of inertia in (kg·m^2), ω is the rotor angular velocity in (rad·s^{-1}).

To simulate the motor start-up, the modified motion equation is used in the Global ODEs and DAEs interface of COMSOL formulated as:

$$\tau = \tau_L + j\frac{\mathrm{d}^2\alpha}{\mathrm{d}t^2}, \tag{7}$$

where α is the rotation angle in (rad).

Firstly, the simulation has been carried out for the no-loaded motor with the moment of inertia of the drive assembly equal to 0.05 kg·m^2 and then for the no-loaded motor unassigned into the drive assembly, so only with the motor moment of inertia equal to

0.012 kg·m^2. Equation (6) and Eq. (7) for the load torque τ_L equal to 0 are:

$$\tau = J\frac{\mathrm{d}\omega}{\mathrm{d}t}, \tag{8}$$

$$\tau = J\frac{\mathrm{d}^2\alpha}{\mathrm{d}t^2}, \tag{9}$$

with neglecting the mechanical losses. Thirdly, the simulation has been carried out for the loaded motor with the adjusted nominal torque equal to 27 N·m, constant during the simulation. The results of these simulations are presented below in Simulation Results.

As mentioned above, the motor starting time is the function of motor torque, moment of inertia and load torque. An equation can be derived from Eq. (6), or Eq. (8), respectively, to define the starting time to accelerate from zero to the motor operating speed as follows:

$$t_a = \int_0^n \frac{2\pi J}{60(\tau - \tau_L)}\mathrm{d}n, \tag{10}$$

or respectively:

$$t_a = \int_0^n \frac{2\pi J}{60\tau}\mathrm{d}n, \tag{11}$$

where t_a is the starting time in (s), n is the motor speed in (rpm) derived from the angular velocity ω from the equation:

$$n = \frac{60\omega}{2\pi}. \tag{12}$$

Into motor model, an electrical circuit is implemented which includes sinusoidal voltage source to feed the motor, end winding impedance and an external coupling to provide a connection to the Rotating Machinery, Magnetic interface [18] and [19]. For one stator phase, the electrical circuit is shown in Fig. 5 for which Kirchhoff's voltage law is defined:

$$v = R_{Send}i + L_{Send}\frac{\mathrm{d}i}{\mathrm{d}t} + v_{emf}, \tag{13}$$

where v is the phase voltage in (V), i is the current in the loop in (A), R_{Send} is the resistance of the stator winding overhang in (Ω), L_{Send} is the leakage inductance of the stator winding overhang in (H), v_{emf} are the induced voltages in (V) across the sides of the all stator coils in one phase, which are implemented in the Rotating Machinery, Magnetic interface. The parameters R_{Send} and L_{Send} are defined in [20].

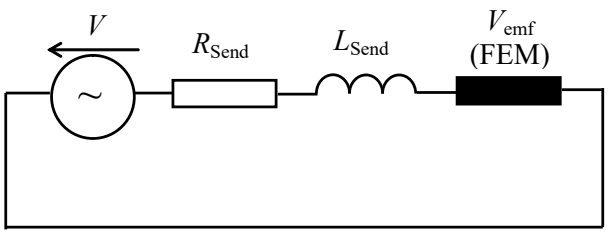

Fig. 5: External stator electrical circuit for one phase.

A part of external rotor electrical circuit is in Fig. 6.

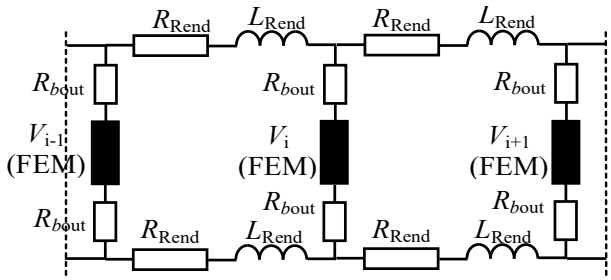

Fig. 6: Part of external rotor electrical circuit.

The voltage equation for one loop of the rotor electrical circuit in Fig. 6 defined by Kirchhoff's voltage law is as follows:

$$v_i - v_{i+1} = 2R_{\mathrm{bout}}i_{\mathrm{b}i+1} + 2R_{\mathrm{Rend}}i_{\mathrm{R}i} + 2L_{\mathrm{Rend}}\frac{\mathrm{d}i_{\mathrm{R}i}}{\mathrm{d}t}, \tag{14}$$

where v_i, v_{i+1} are the voltages of two neighbouring bars in (V), which are implemented in the Rotating Machinery, Magnetic interface, $i_{\mathrm{b}i}$, $i_{\mathrm{b}i+1}$ are the currents in the bars in (A), $i_{\mathrm{R}i}$, $i_{\mathrm{R}i+1}$ are the currents in the rings in (A), R_{bout} is the resistance of the part of bar, which is outside of the rotor iron in (Ω), R_{Rend} is the resistance of the rotor end-ring segment in (Ω), L_{Rend} is the leakage inductance of the rotor end-ring segment in (H). The parameters R_{bout}, R_{Rend} and L_{Rend} are defined in [20].

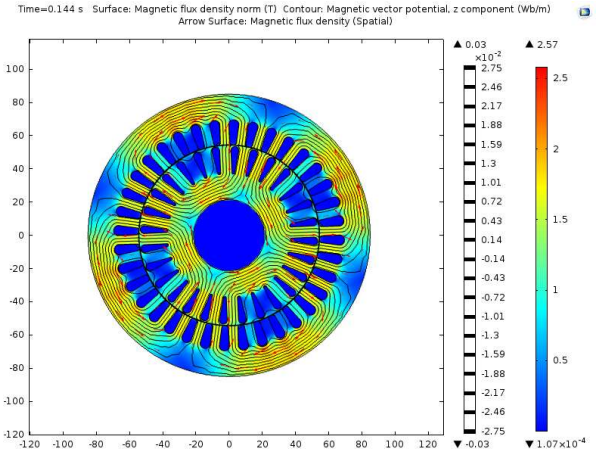

Fig. 7: Magnetic flux density and equipotential lines of magnetic vector potential.

To design the motor model in COMSOL, the manufacturer's layouts of the stator and rotor sheets were used. The induction motor geometry with the magnetic flux density and equipotential lines of magnetic vector potential is shown in Fig. 7 at the motor operating speed.

4. Simulation Results

To compare measured courses of the stator currents, torque and speed of the induction motor in the drive assembly and the moment of inertia equal to 0.05 kg·m^2 were adjusted into COMSOL. The results are in Fig. 8, Fig. 9, and in Fig. 10, respectively. Moreover, the courses of the rotor bar and ring currents are shown in Fig. 11 and in Fig. 12.

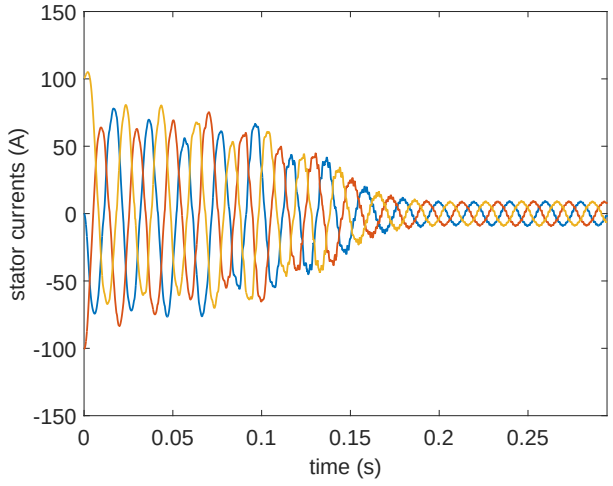

Fig. 8: Waveform of stator currents (no-loaded motor, $J = 0.05$ kg·m^2).

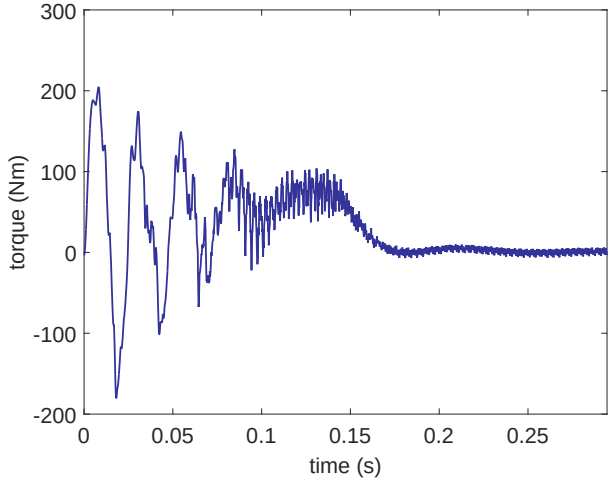

Fig. 9: Waveform of inner torque (no-loaded motor, $J = 0.05$ kg·m^2).

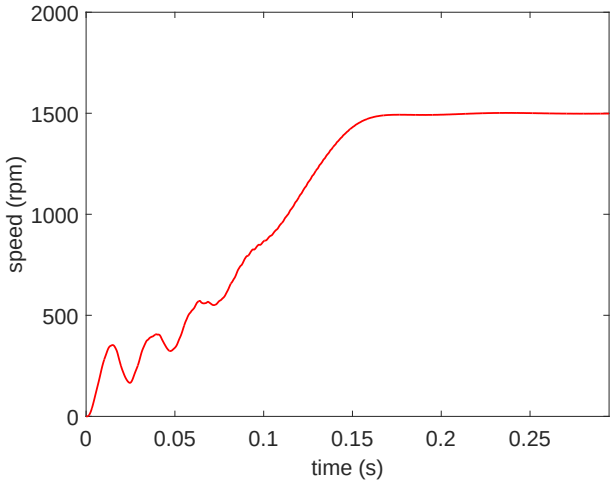

Fig. 10: Waveform of speed (no-loaded motor, $J = 0.05$ kg·m^2).

As seen from the simulated waveforms, the motor starting time is close to 0.2 s and it is comparable to the starting time detected from the experimental measurement. The start-up is accompanied by the high starting currents, which reach the peak value c. 100 A at the time of the motor connection. This value corresponds to the one from the measurements as can be seen in Fig. 2. The simulated and measured courses of the stator currents including the values of starting currents are very close as it can be seen in Fig. 2 and Fig. 8. The transient process from the motor standstill to the time equal to c. 100 ms is accompanied by oscillations of the simulated torque in comparison to the measured course, which corresponds to the oscillations of the currents in the rotor bars and rings, as seen in Fig. 11 and Fig. 12, respectively. These oscillations are given by behaviour of the model in COMSOL software. The frequency range of the measured dynamic torque of the used torque transducer is limited by the

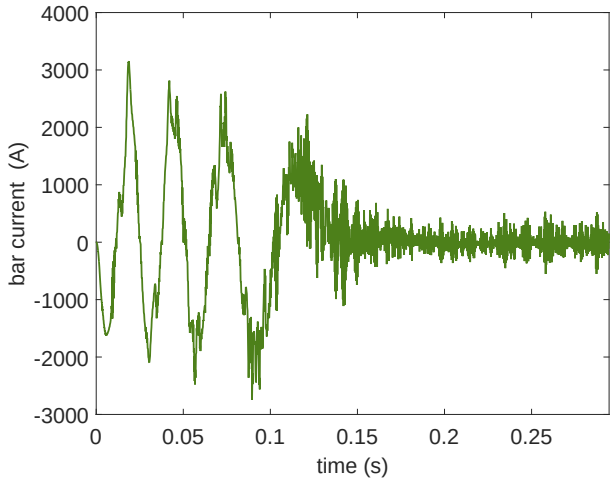

Fig. 11: Waveform of bar current (no-loaded motor, $J = 0.05$ kg·m^2).

natural frequency of the mechanical measuring system and by the cut-off frequency of transducer electronics (200 Hz).

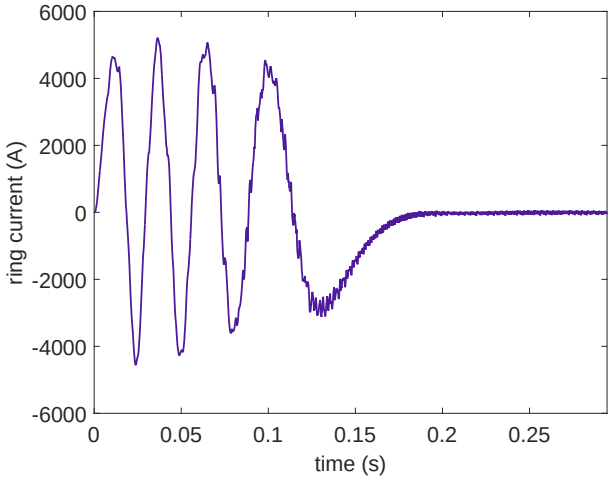

Fig. 12: Waveform of ring current (no-loaded motor, $J = 0.05$ kg·m^2).

In the case when the motor is unassigned into the drive assembly, only its moment of inertia equal to 0.012 kg·m^2 was adjusted into COMSOL. The motor inner torque during its starting is in Fig. 13 and motor speed in Fig. 14. The start-up is very fast with oscillations both in torque and speed before reaching the steady-state. These oscillations are less damped due to c. four times lower moment of inertia in comparison to the previous simulation shown in Fig. 9 and Fig. 10, respectively. As a result of the lower moment of inertia, the motor reaches its no-load speed faster, but the time for reaching the steady state is longer. The oscillation frequency of the motor speed is lower c. two times in comparison to the one when the motor is in the drive assembly (see Fig. 10).

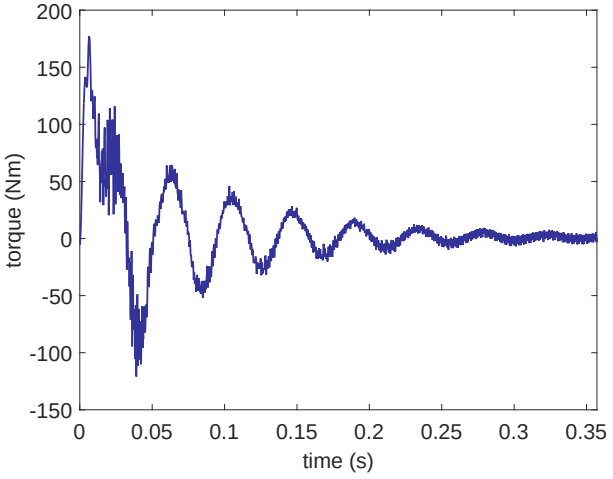

Fig. 13: Waveform of inner torque (no-loaded motor, $J = 0.012$ kg·m^2).

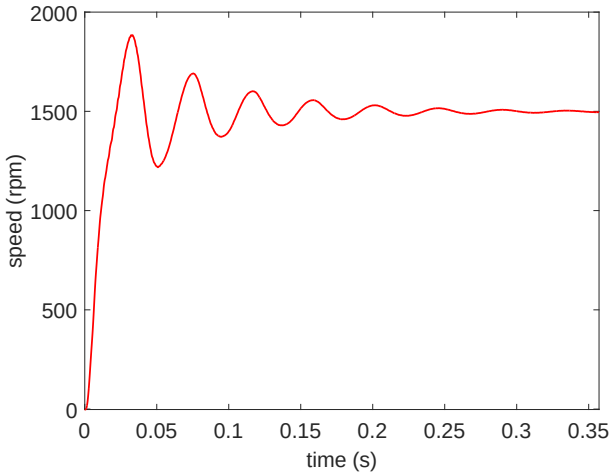

Fig. 14: Waveform of speed (no-loaded motor, $J = 0.012$ kg·m^2).

In the last case, the simulation of the motor start-up has been carried out for the nominal torque equal to

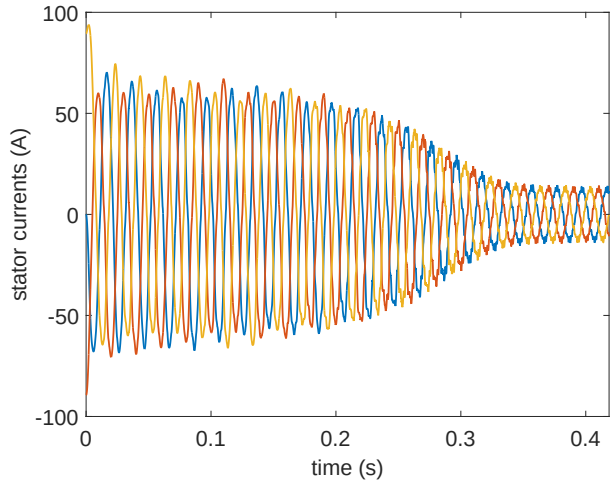

Fig. 15: Waveform of stator currents (nominal load).

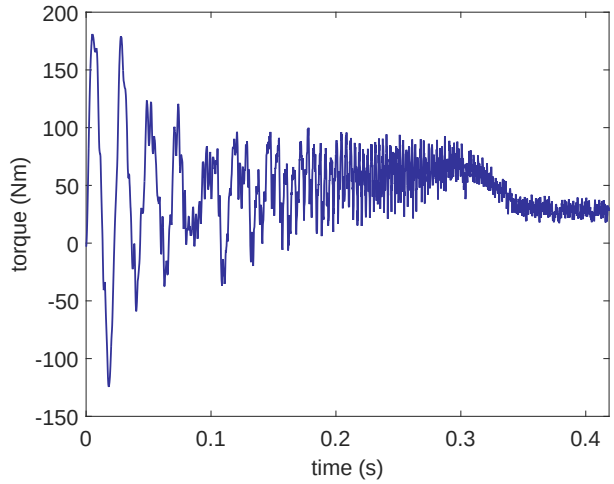

Fig. 16: Waveform of inner torque (nominal load).

27 N·m. Stator currents are shown in Fig. 15, motor inner torque in Fig. 16, motor speed in Fig. 17, current in the rotor bar in Fig. 18, and current in the rotor ring in Fig. 19.

As can be seen from the simulated waveforms of stator currents, torque or speed, the motor reaches its steady-state after time equal to c. 0.35 s. The start-up is also accompanied by the oscillations in the motor inner torque, which are lower when the motor is loaded. The oscillation frequency of the motor speed is close to the one in Fig. 10. The rate of speed rise is c. 2.6 times lower than in the case of the no-loaded motor. A comparison of the stator current, motor torque and speed from the simulation to the ones from the motor catalogue shown in Tab. 1 is presented in Tab. 2. In Tab. 3, a comparison of measured and simulated stator current and motor speed of the no-loaded motor in the steady-state is shown.

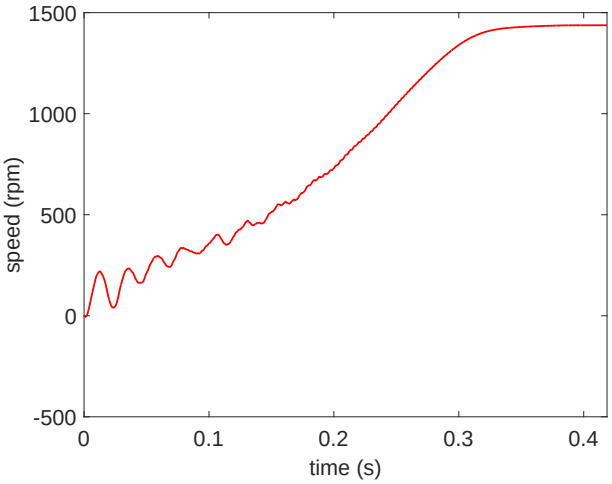

Fig. 17: Waveform of speed (nominal load).

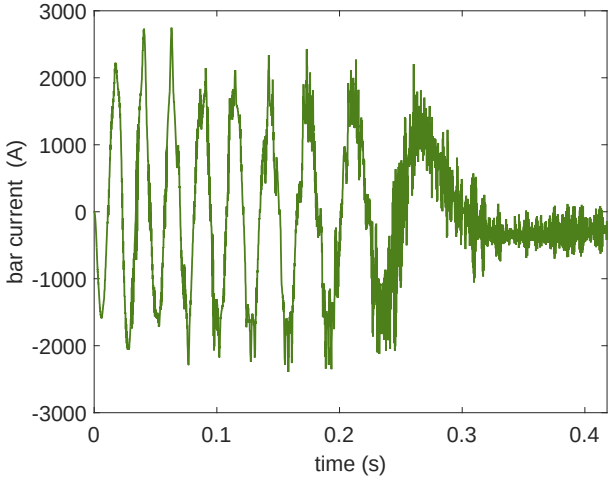

Fig. 18: Waveform of bar current (nominal load).

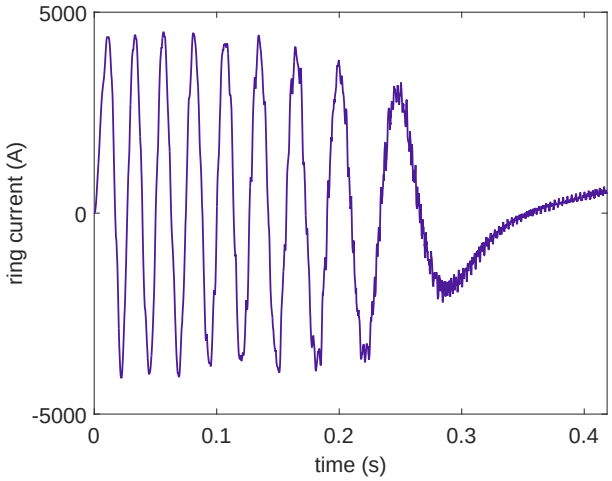

Fig. 19: Waveform of ring current (nominal load).

Tab. 2: Comparison of the chosen motor steady-state parameters for the nominal load.

	Stator current	Torque	Speed
Motor catalogue	8.4 A	27 N·m	1440 rpm
Simulation	8.6 A	27.6 N·m	1437.5 rpm

Tab. 3: Comparison of the chosen motor steady-state parameters for the no-load operation.

	Stator current	Speed
Measurement	5.7 A	1500 rpm
Simulation	5.5 A	1498.5 rpm

5. Conclusion

As can be seen from Tab. 2 and Tab. 3, the chosen simulated motor parameters match the ones from the measurement, or the nameplate ones respectively, very well. The starting current ratio from the motor catalogue is equal to 6, which conforms to the starting current of 50.4 A. As detected from the measured phase currents, the average value of three-phase currents just after starting is equal to c. 60 A, whereas the one from the simulation is equal to c. 56 A. A comparison of the torque during motor start-up is limited due to the used type of torque transducer as mentioned above, and by the fact that the inner electromagnetic torque is simulated, whereas the mechanical (shaft) torque is measured. The starting time of the no-loaded motor detected both from measurement and from the simulation is comparable as declared above. As expected, it is longer when the motor is loaded as can be seen from Fig. 15.

It is evident from the start-up motor simulations that the torque and speed courses are dominantly influenced by the rotor bar currents and the variable rotor frequency during motor starting, and after achieving the

motor stable speed mainly by the stator currents and by the constant stator frequency.

It should be noted that the simulated values depend on the accuracy of identification and calculation of the induction motor parameters used in its model, on the geometry of motor iron sheets and material properties, on the proper meshing of the motor air gap, and on the adjusted time step of the simulation.

Acknowledgment

This work was supported by the SGS, Faculty of Electrical Engineering and Computer Science, VSB–Technical University of Ostrava under Grant No. SP 2017/152.

References

[1] Starting and control of three-phase asynchronous motors. In: *Moeller* [online]. 2017. Available at: https://www.scribd.com/document/69903503/Moeller-Starting-and-Control-of-\Three-phase-Asynchronous-Motors.

[2] AC motors starting and protection systems. In: *Schneider Electric* [online]. 2017. Available at: http://www.schneider-electric.hu/documents/automation-and-control/asg-4-motor-starting-and-protection.pdf.

[3] Basic technical information about low voltage standard motors. In: *ABB Motor guide* [online]. 2014. Available at: http://new.abb.com/docs/librariesprovider53/about-downloads/low-voltage-motor-guide.pdf?sfvrsn=2.

[4] PETROV, G. N. *Elektricke stroje 2, asynchronni stroje-synchronni stroje*. Praha: Academia, 1982.

[5] MRAVEC, R. *Elektricke stroje a pristroje I. Elektricke stroje*. Praha: SNTL, 1979.

[6] COHEN, V. Induction motors-protection and starting. In: *CBI electric low voltage* [online]. 2000. Available at: http://cbi-lowvoltage.co.za/sites/default/files/downloads/TechPapers/Motor.pdf.

[7] SIMOTICS low-voltage motors. In: *Siemens AG* [online]. 2014. Available at: https://www.industry.usa.siemens.com/drives/us/en/electric-motor/nema-motors/Literature-and-technical-resources/Documents/Catalog%20D81-1_2014_English.pdf.

[8] GOH, H. H., M. S. LOOI and B. C. KOK. Comparison between direct-on-line, star-delta and auto-transformer induction motor starting method in terms of power quality. *Lecture Notes in Engineering and Computer Science*. 2009, vol. 2, iss. 1, pp. 1558–1563. ISSN 2078-0958.

[9] AC induction motor fundamentals. In: *Microchip Technology Inc.* [online]. 2003. Available at: http://ww1.microchip.com/downloads/en/AppNotes/00887a.pdf.

[10] GARG, A. and A. TOMAR. Starting time calculation for induction motor. *Journal of Electrical & Electronic Systems*. 2015, vol. 5, iss. 5, pp. 56–60. ISSN 2332-0796. DOI: 10.4172/2332-0796.1000149.

[11] KARMAKAR, S., S. CHATTOPADHYA, M. MITRA and S. SENGUPTA. *Induction motor fault diagnosis: approach through current signature analysis*. 1st ed. Singapore: Springer, 2016. ISBN 978-981-10-0623-1.

[12] FINLEY, W. R. Troubleshooting induction motors. In: *IAS Annual Meeting (IEEE Industry Applications Society)*. Rome: IEEE, 2000, pp. 3491–3498. ISBN 0-7803-6402-3. DOI: 10.1109/IAS.2000.882669.

[13] MARTINEZ, J., A. BELAHCEN and A. ARKKIO. A 2D FEM model for transient and fault analysis of induction machines. *Przeglad Elektrotechniczny*. 2012, vol. 88, iss. 7B, pp. 157–160. ISSN 0033-2097.

[14] BHAGAT, V. K. and H. C. PATEL. Electromagnetic analysis of induction motor using FEM. *Journal of Emerging Technologies and Innovative Research*. 2014, vol. 1, iss. 7, pp. 903–908. ISSN 2349-5162.

[15] BIANCHI, N., S. BOLOGNANI and G. COMELATO. Finite element analysis of three-phase induction motors: comparison of two different approaches. *IEEE Transactions on Energy Conversion*. 1999, vol. 14, iss. 4, pp. 1523–1528. ISSN 0885-8969. DOI: 10.1109/60.815100.

[16] KOCMAN, S., P. PECINKA and T. HRUBY. Induction motor modelling using COMSOL Multiphysics. In: *17th International Scientific Conference on Electric Power Engineering*. Prague:

IEEE, 2016, pp. 408–412. ISBN 978-150900907-7. DOI: 10.1109/EPE.2016.7521727.

[17] COMSOL Multiphysics. *Reference manual*. Comsol, 2013.

[18] SAVOV, V. N., Z. D. GEORGIEV and E. S. BOGDANOV. Analysis of cage induction motor by means of the finite element method and coupled system of field, circuit and motion equations. *Electrical Engineering*. 1997, vol. 80, iss. 1, pp. 21–28. ISSN 0948-7921.

[19] DE GERSEM, H., K. HAMEYER and T. WEILAND. Field-circuit coupled models in electromagnetic simulation. *Journal of Computational and Applied Mathematics*. 2004, vol. 168, iss. 1–2, pp. 125–133. ISSN 0377-0427. DOI: 10.1016/j.cam.2003.05.008.

[20] KOCMAN, S., T. HRUBY, P. PECINKA and A. NEUMANN. FEM model of asynchronous motor for analysis of its parameters. In: *11th International Conference on ELEKTRO 2016*. Strbske Pleso: IEEE, 2016, pp. 315–319. ISBN 978-146738698-2. DOI: 10.1109/ELEKTRO.2016.7512088.

About Authors

Stanislav KOCMAN was born in Brno, the Czech Republic. He received his M.Sc. degree from Brno University of Technology in 1987 and Ph.D. and Assoc. Prof. degrees from VSB–Technical University of Ostrava in 2004 and in 2008, respectively. His research interests include power quality, power efficiency of the electrical drives and modelling of electrical machines.

Petr ORSAG was born in Prerov, the Czech Republic. He received his M.Sc. and Ph.D. degrees from the VSB–Technical University of Ostrava in 1988 and in 1999, respectively. His research interests include electromechanical systems diagnostics, power efficiency of the electrical drives and modelling of electrical machines.

Pavel PECINKA was born in Celadna, the Czech Republic. He received B.Sc. and M.Sc. degrees from the Faculty of Electrical Engineering and Computer Science, VSB–Technical University of Ostrava in 2012 and in 2014, respectively. He currently works towards his Ph.D. degree. His research interests include electric machines and devices, power electronics and simulations using finite element method.